Optica Applicata, Vol. XXXI, No. 2, 2001

Polarisation behaviour of different fiber-optic interferometer configurations under temperature changes

LESZEK R. JAROSZEWICZ

Institute of Applied Physics, Military University of Technology, ul. Kaliskiego 2, 00–908 Warsaw 49, Poland.

The paper deals with presents the theoretical investigation into the influence of temperature on the fiber-optic interferometer action for different configuration of the latter. Based on the phenomenological description of interference phenomena in the optical fiber, the role of coherence and polarisation in the fiber-optic interferometer is discussed. The final conclusions are used in the main part of the paper connected with an analysis of temperature influence on the action of different fiber-optic interferometer configurations. This analysis is based on the Jones matrix formalism applied to interferometers of minimal functional configuration. Finally, it is suggested using the fiber-optic ellipsometer for polarisation controlling.

1. Introduction

The development of the cheap single-mode optical fibres and related in-line elements in the eighties caused the detailed fiber-optic interferometer investigation. Those systems are designed for sensor application mainly due to their extremely high sensitivity [1]. Additionally, using optical fibers makes such a device free from the dust problem existing in a common bulk configuration. Then, in the last two decades, fiber-optic analogues of the classical interferometric systems have been proposed [2]. However, the properties of optical fiber used to construct such a system introduce significant modifications to the system action.

The main problem is connected with the fact that the commonly used, single -mode optical fiber has birefringent properties [3], thus gives polarisation influence on interference phenomena. Generally, those effects are well known as Fresnel –Arago's condition [4], but in the bulk interferometer this aspect is commonly neglected because it uses isotropic property of free space for beam propagation. For the above reason, a suitable analytical description of interference phenomena in optical fiber is presented in the next section. The results obtained were used as a general conclusion concerning the main difference between bulk and fiber-optic interferometric devices.

On the basis of these investigations, the influence of temperature on interferometer action is presented as the main part of the paper. The investigation of this

parameter for system action has been selected because vibration and temperature are the main sources of instability of fiber-optic sensor [5], [6]. The environmental vibration is usually high frequency effect that affects noise level and decreases system resolution [7]. This influence can be reduced by perfect fixing or embedding all optical elements in one base. On the other hand, the temperature fluctuation is low frequency effect, which affects directly the drift phenomena [8], [9]. Because its reduction is more difficult than vibration reduction, then its investigation is especially interesting for understanding fiber sensor action. Therefore, in this paper, the fiber-optic interferometric configurations are compared with respect to their resistance to the temperature changes. In order to select the best fiber-optic interferometer, the minimal functional configuration has been used for such a comparison. Finally, it is suggested that the passive fiber-optic ellipsometer should be applied for monitoring the influence of temperature on the state of polarisation (SOP) in interferometer system.

The theoretical considerations provided here are based on Jones matrix calculus [10]. This method is especially interesting to the description of optical system for two reasons. First, it allows maintaining phase information, which is basic for an action of an interferometric system. Second, this method gives clear and lucid description of the effect of individual elements (and/or parameters of those elements) on the form of the system output signal. Moreover, recent development of computer software allows us to obtain at least visualised results of numerical calculations describing the giving system, if not simple analytical expressions.

2. Phenomenological description of interference phenomena in optical fiber

Since the angular size of the optical source along a single-mode optical fiber is constant (*i.e.*, equal to the fiber numerical aperture), the spatial coherence is preserved in the transverse cross-section along the fiber [11], [12]. This is the first difference between the fiber-optic and bulk interference. In the latter system, the spatial coherence changes along optical way. Therefore, the time coherence and polarisation effects on interference phenomena in optical fiber should be analysed. Such an analysis based on phenomenological approach has been presented in [13], and here only a short review concerning the final results is provided.

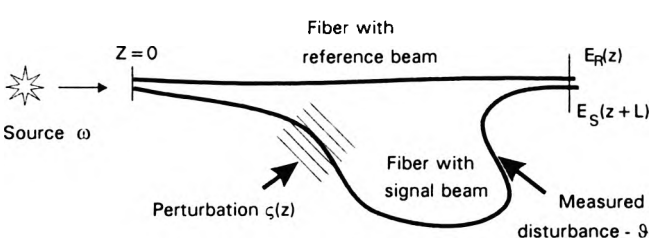

Fig. 1. Schematic representation of fiber-optic interference phenomena.

A schematic view of fiber-optic interference phenomena is shown in Fig. 1. The light beams interacting in a single-mode fibre will be treated as quasi-monochromatic plane waves (actually, they have the Gaussian spatial field distribution). Moreover, it will be assumed that only the signal wave is perturbed (and not the reference one).

The two waves interacting at the point z can be described by the following Jones vectors [10]:

$$E_R = \begin{bmatrix} E_x \\ E_y e^{i\delta} \end{bmatrix} e^{i[\omega t-(\beta_0-\beta_1)z]}, \tag{1}$$

$$E_S = \mathbf{R}[\varphi+\eta]\begin{bmatrix} E_x \\ E_y e^{i(\delta+\varkappa+\varepsilon)} \end{bmatrix} e^{i[\omega t-\beta_0(z+L)-\beta_1(z+L)+\vartheta+\zeta]}. \tag{2}$$

In this notation, the reference wave (1) is the plane wave with an elliptical SOP characterised by the amplitudes of x- and y-components (E_x and E_y) and the relative phase retardation δ. Additionally, the propagation constant $\beta = \beta_0+\beta_1$ is assumed to be the sum of the propagation constant β_0 at the central frequency ω_0 of source radiation ($\beta_0 = \omega_0/v_p$, v_p – phase velocity) and the "dispersion" propagation constant ($\beta_1 = (\omega-\omega_0)/v_g$, v_g – group velocity) connected with spectral source width $\delta\omega$ ($\omega_0 \gg \delta\omega$). All the differences and disturbances are included in the signal wave (2). This wave contains a parameter L – the differences in the lengths of fiber-optic arms, and a group of averaged (*i.e.*, constant) quantities: $\varkappa$ – changes in phase retardation between field components, φ – the angle of polarisation plane rotation ($\mathbf{R}[\varphi]$ – the rotation matrix), and ϑ – the phase shift induced by the measured effect. These values can be treated as the integrals

$$\mathscr{R} = \int_{z_1}^{z_2} \mathscr{I}(z)\mathrm{d}z, \quad \mathscr{R} = \varkappa, \varphi, \vartheta \tag{3}$$

where z_1-z_2 is the fiber length on which the influence $\mathscr{I}$ exists.

Additionally, the signal wave (2) also also the following perturbation parameters, the probability distributions of which are connected with the source spectral distribution: η – perturbation of the polarisation azimuth, ε – perturbation of the phase retardation between field components, ζ – the perturbation of the phase shift. In the first approximation, it was assumed that those perturbations depend linearly on the source spectral distribution ($\eta = \Xi(\omega)\varphi$, $\varepsilon = \Xi(\omega)\varkappa$, $\zeta = \Xi(\omega)\vartheta$, where $\Xi(\omega) = (\omega-\omega_0)/\omega_0$), and and they are independent random variables.

The light intensity resulting in interference phenomena is as follows [4]:

$$I = \langle (E_R+E_S)(E_R+E_S)^* \rangle \tag{4}$$

where the symbol $\langle \ldots \rangle$ means averaging in time due to the source spectral distribution.

For the multi-mode Gaussian model source, containing the finite number $(2n+1)$ of single peaks, each characterized by the spectral distribution g_i, the central

frequency ω_i and the full width at half maximum (FWHM) $\delta\omega_i$ [13]

$$g = \sum_{i=-n}^{n} a_i g_i, \quad a_i > 0, \quad \sum_{i=-1}^{n} a_i = 1, \quad \int g_i(\omega)\mathrm{d}\omega = 1, \tag{5}$$

the final relation for interference phenomena in optical fiber is

$$I = 2 + 2T(\varphi)T(\vartheta)\left\{\left[\sum_{i=-1}^{n}(E_x^2\cos(\vartheta-\beta_i L)+E_y^2 T(\varkappa)\cos(\vartheta+\varkappa-\beta_i L)t_i\left(\frac{\omega_i}{v_{gi}}L\right)\right]\cos\varphi\right.$$

$$\left.+E_x E_y\left[\sum_{i=-1}^{n}(\cos(\vartheta-\delta-\beta_i L)+T(\varkappa)\cos(\vartheta+\varkappa+\delta-\beta_i L)t_i\left(\frac{\omega_i}{v_{gi}}L\right)\right]\sin\varphi\right\} \tag{6}$$

where:

$$T(\chi) = \sum_{i=-1}^{n} t_i(\chi), \quad t_i = a_i \exp\left(-\frac{\delta\omega_i^2}{16\ln 2\omega_i^2}\chi^2\right), \tag{7}$$

and $\beta_i = nk_i$ is the propagation constant of the i-th source wavelength in optical fiber.

The above relation contains open dependence of fiber-optic interference on coherence as well as SOP of interacting waves. They can be used for analysis of mutual relationship between those two phenomena, as shown in [13], where the interpretation of Fresnel–Arago's experiments is presented. Generally, considering the application of the phenomenon in question to investigation of the sensor, the latter result (6), can be rewritten as [14]

$$I = I_0\{1 + V(\gamma, \mathrm{SOP})\cos[\vartheta - \alpha(\gamma, \mathrm{SOP})]\} \tag{8}$$

where fringe visibility V and bias α are dependent on source coherence γ and mutual polarisation of interacting waves (SOPs).

Taking into consideration the source with spectrum described by Eq. (5), each mode of which has the same FWHM $\delta\omega$ separated by the same distance ($\omega_{i+1} - \omega_i = m\delta\omega$), where $m\delta\omega \ll \omega_0$, and assuming linear polarisation of both interacting beams ($E_x = E_y = 1/\sqrt{2}$) and $\varphi = \varkappa = \delta = 0$) from Eq. (6) we have

$$I = 2[1 + T(\vartheta)T\left(\frac{\omega_0}{v_g}L\right)\sum_{i=-n}^{n} a_i\cos(\vartheta - \beta_i L)]. \tag{9}$$

The numerically obtained visibility of this interference relation for classic He-Ne laser operating at a wavelength of 632.8 nm with nine modes and for two different peak separations ($m = 4$ and $m = 5$) as well as for single-mode is shown in Fig. 2.

As one can see, the measurable contrast in the optical fibre interferometer is achieved by suitable choose of the optical path difference L between the interferometer arms. It is the same relation as for the bulk interferometer – if the path difference is smaller than the source coherence, then interference exists [4]. Moreover, it is worth noting that in the fiber-optic technique, precisely adjustment of fiber lengths to obtain maximum interference visibility can be easily achieved using the fiber-optic stretcher based on a piezoceramic transducer [15].

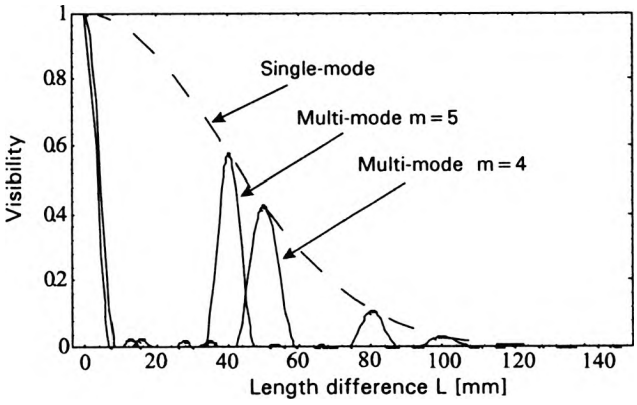

Fig. 2. Intensity as a function of optical path difference L for the nine-mode He-Ne laser with $\delta\omega = 6.3$ MHz and double peak separation $m = 4$ and $m = 5$ and for single-mode source (dashed line), [14].

In the case, when the interacting beams passing through the fibers of equal length ($L = 0$) and the source used is monochromatic with frequency ω_0, then from Eq. (6) the resulting light intensity may be expressed as follows [14]:

$$I = 2 + 2\{[E_x^2 \cos\vartheta + E_y^2 \cos(\varkappa + \vartheta)]\cos\varphi + E_x E_y [\cos(\vartheta - \delta)\cos(\varkappa + \delta + \vartheta)]\sin\varphi]\}. \tag{10}$$

Then the interference strongly depends on mutual polarisation of interacting beams. This is the main problem with the for fiber-optic system because even if the parameters connected with initial SOP of incoming light beams (E_x, E_y, δ) are fixed, the parameters $\varkappa$, φ generally representing changes of fiber birefringence will affect interference phenomena. This polarisation effect on fiber-optic interferometers of different types has been investigated in [16]. Nevertheless, the dependence of both the fiber birefringence and different interferometry configurations on temperature should be investigated.

3. Influence of temperature on polarisation behaviour in optical fiber

It is well known that the single-mode optical fiber guides two degenerated modes HE_{11}^x, HE_{11}^y that are linear, perpendicularly polarised and have equal propagation constants ($\beta_x = \beta_y$) [17]. However, any elastic deformation introducing perturbation in circular geometry of fiber core or circular symmetry of refractive index distribution across the fiber, decouples those modes ($\beta_x \neq \beta_y$). Such a fiber has birefringence properties ($\Delta\beta = |\beta_x - \beta_y|$) [18], [19]. A general analytical description of this fiber can be made in terms of Kapron rule of equivalence [20]. In essence, the Kapron equivalence states that any unknown optical system or medium with regard to its effects upon polarised light can always be equivalent to a trio of basic discrete

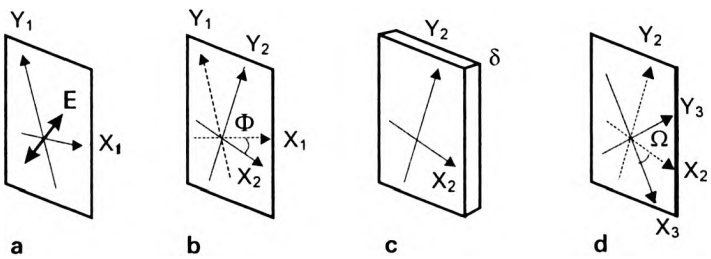

Fig. 3. Illustration of the Kapron rule of equivalence: **a** – the light input and its reference axes $X_1 - Y_1$, **b** – the rotation of the axes by an angle Φ to the axis of linear phase retarder $X_2 - Y_2$, **c** – the linear retarder of δ retardation, **d** – the output light after passage through a retarder undergoes additional axis rotation of Ω angle [16].

devices: a rotation of the axis (inclination) Φ, a linear retarder (with phase retardation δ), and circular retarder (with axis rotation Ω), as shown in Fig. 3.

The above rule has the following form [17] in the Jones matrix formalism [3]

$$\mathbf{M} = \mathbf{R}[\Omega - \Phi]\,\mathbf{G}[\delta]\mathbf{R}[\Phi] \tag{11}$$

where in the Cartesian system the rotation matrix **R** and the retardation matrix **G** have the following form:

$$R(\theta) \equiv \begin{bmatrix} \cos\theta & -\sin\theta \\ \sin\theta & \cos\theta \end{bmatrix},$$

$$\mathbf{G}(\delta) \equiv \begin{bmatrix} \exp(-i(\delta/2)) & 0 \\ 0 & \exp(i(\delta/2)) \end{bmatrix}. \tag{12}$$

The standard single-mode fiber used in interferometer is mechanically deformed during interferometer construction. Thus, assuming that interferometer arm length L has resultant fiber twist per unit length ϕ_t and resultant retardation δ with main birefringence axes oriented at an angle Φ with respect to co-ordinate system, the final form of its Jones matrix can be re-written on the basis of [21] as

$$\mathbf{M} = \mathbf{D}[\phi]\cdot\mathbf{R}[\phi_R - \Phi]\cdot\mathbf{G}[\phi_G]\cdot\mathbf{R}[\Phi] \tag{13}$$

where: $\phi = nk_0L$, $\phi_R = \varkappa_t L$, $\phi_G = \Delta nk_0 L$ [18]. Additionally, $\mathbf{D}[\phi] = \exp(-i\phi)\mathbf{I}$ is the matrix represented constant phase retarder, where **I** is the unitary matrix describing isotropic medium, $nk_0 = (\beta_x + \beta_y)/2$ is the mean value of propagation constant, $\Delta nk_0 = \Delta\beta$ and $\varkappa_t$ are the optical linear and circular birefringence induced by deformation, respectively. The first and the last two components of this relation represent the phase shift ϕ of light wave propagating through the single-mode standard and birefringent fibers, respectively, while the second matrix connected with fiber twist represents rotation of SOP azimuth.

It has been experimentally confirmed that fluctuations of the optical phase passing through an optical fiber are generated mainly by the atmospheric tem-

perature fluctuations [22]. It should be mentioned that in interferometric interaction according to Eq. (4) the above optical phase fluctuations represent phase value averaged over the time period equal to interaction time Δt. However, because the temperature fluctuations are usually slowly time varying [9], their changes over interaction time Δt might be neglected, *i.e.*

$$\langle \phi[t, T(t)+\Delta T(t)] \rangle \stackrel{\text{def}}{=} \frac{1}{\Delta t} \int_{t}^{t+\Delta t} \phi[t, T(t)+\Delta T(t)]\,\mathrm{d}t = \phi(T+\Delta T). \tag{14}$$

Thus, the optical phase fluctuations with temperature changes ΔT can be written in the first approximation as

$$\phi(T+\Delta T) = \phi(T)+\frac{\mathrm{d}\phi}{\mathrm{d}T}\,\Delta T \tag{15}$$

where $\mathrm{d}\phi/\mathrm{d}T$ is dependent on the type of optical fiber.

The phase changes with temperature for standard single-mode fiber are due to two effects. The first one is the change in fiber length due to thermal expansion or contraction, and the second one is the temperature-induced change of the refractive index. Hence, since $\phi = nk_0L$, one can write [5]

$$\frac{\mathrm{d}\phi}{\mathrm{d}T} = \frac{d(nk_0L)}{\mathrm{d}T} = k_0\left(n\frac{\mathrm{d}L}{\mathrm{d}T}+L\frac{\mathrm{d}n}{\mathrm{d}T}\right) = k_0(n\delta L_T + L\delta n_T) \tag{16}$$

where: $\delta L_T = 5\times 10^{-7}/^{\circ}\mathrm{Cm}$, $\delta n_T = 1\times 10^{-5}/^{\circ}\mathrm{Cm}$ for silica fiber with $n = 1.456$ and $\lambda = 0.632\times 10^{-6}$ m [23]. Value for the thermal expansion coefficient and the temperature-dependent refractive index can vary significantly for multicomponent glasses [9]. Moreover, δn_T is itself a function of temperature and wavelength, and most tabulated values are averaged over a large temperature range and given for only a few wavelengths. Nevertheless, the above value will be used in numerical calculation in the following part of the paper.

In the case of linear birefringence induced in single-mode fiber, the temperature sensitivity of phase $\phi_G = \Delta n k_0 L$ is given by the relation [24]

$$\frac{\mathrm{d}\phi_G}{\mathrm{d}T} = \frac{d(\Delta n k_0 L)}{\mathrm{d}T} = k_0\left(\frac{\Delta n}{n}\frac{\mathrm{d}n}{\mathrm{d}T}\,L + \Delta n\frac{\mathrm{d}L}{\mathrm{d}T}\right). \tag{17}$$

Since the second term in (17) is smaller by two orders of magnitude than the first one, it can be neglected and the equation becomes [25]

$$\frac{\mathrm{d}\phi_G}{\mathrm{d}T} = k_0\frac{\Delta n}{n}\frac{\mathrm{d}n}{\mathrm{d}T}L = k_0\frac{\Delta n}{n}\,\delta n_T L = \frac{2\pi}{nL_B}\,\delta n L \tag{18}$$

where $L_B = \lambda/\Delta n$ is acharacteristic parameter of fiber birefringence named the beat length.

Finally, for circular birefringence induced in single-mode fiber, the temperature sensitivity of phase $\phi_R = \varkappa_t L$ can be expressed as

$$\frac{d\phi_R}{dT} = \frac{d(\varkappa_t L)}{dT} = \frac{d(2GC\phi_t L/n)}{dT} = -\frac{1}{n^2} 2GC\phi_t L\delta n_T \tag{19}$$

where: $G = 3.27 \times 10^{10}$ N/m^2 is a rigidity modulus, $C = 3.51 \times 10^{-12}$ m^2/N is a photoelastic constant for silica fiber [26], and $\phi_t L = \chi$ is total fiber twist a thermal independent parameter.

Thus, using relations (15)–(19) the matrix **M** of fiber-optic interferometer arm vs. temperature changes ΔT can be expressed as

$$\mathbf{M}(\Delta T) = \mathbf{D}[\phi(\Delta T)]\mathbf{R}[\phi_R(\Delta T) - \Phi]\mathbf{G}[\phi_G(\Delta T)]\mathbf{R}[\Phi]$$

where:

$$\phi(\Delta T) = \phi + \frac{d\phi}{dT}\Delta T = k_0[nL + (n\delta L_T + L\delta n_T)\Delta T], \tag{20a}$$

$$\phi_R(\Delta T) = \phi_R + \frac{d\phi_R}{dT}\Delta T = 2GC\frac{\chi}{n}\left(1 - \frac{\delta n_T}{n}\Delta T\right), \tag{20b}$$

$$\phi_G(\Delta T) = \phi_G + \frac{d\phi_G}{dT}\Delta T = 2\pi\frac{L}{L_B}\left(1 + \frac{\delta n_T}{n}\Delta T\right). \tag{20c}$$

The light wave passing through such a fiber has the SOP described in the Jones formalism as a vector [10]

$$E_{\text{out}} = \mathbf{M}(\Delta T)E_{\text{in}} \tag{21}$$

where

$$E_{\text{out}} = \begin{bmatrix} E_x \\ E_y e^{i\sigma} \end{bmatrix}, \quad E_{\text{in}} = \begin{bmatrix} \cos\theta \\ \sin\theta e^{i\delta} \end{bmatrix} \tag{21a,b}$$

is the so-called standard Jones vector of plane wave from which the two main parameters describing the SOP, the azimuth Θ and the ellipticity ε, can be obtained at any point along fiber as [27]:

$$\Theta = \frac{1}{2}\arctan\left[\frac{2\text{Re}(X)}{1-|X|^2}\right], \quad \varepsilon = \frac{1}{2}\arcsin\left[\frac{2\text{Im}(X)}{1-|X|^2}\right] \tag{22}$$

where $X = \dfrac{E_y}{E_x}e^{i\sigma}$.

Thus, from relations (20)–(22) one can see that in optical fiber used for interferometer construction temperature generates changes of the polarisation azimuth (via matrix **R**) as well as the polarisation ellipticity (via matrix **G**). Moreover, for birefringent fiber described by (20), the thermal dependence of fiber circular birefringence influences ellipticity changes, whereas the thermal dependence of fiber linear retardation influences azimuth changes, as shown in Fig. 4. The linearly polarised input light and the main axis of linear retarder equal $\pi/4$ ($\Phi = \pi/4$) are assumed in simulation.

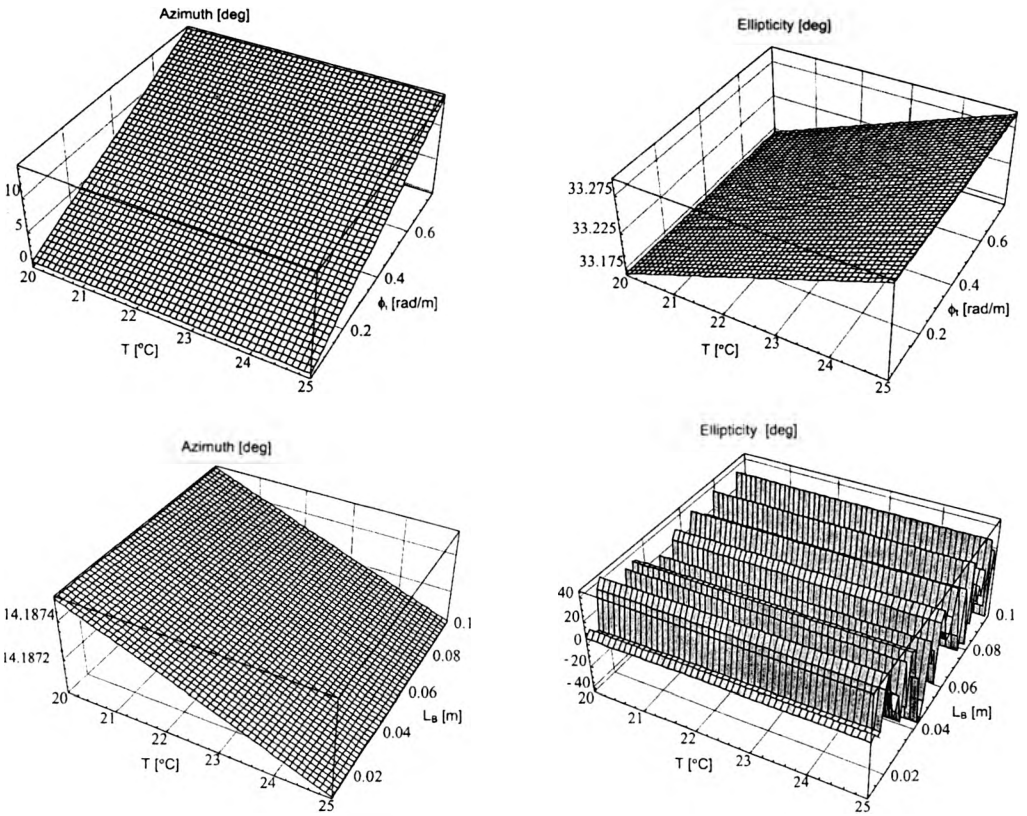

Fig. 4. Temperature effects on the SOP of the fiber-optic interferometer arm for changes of fiber twist rate ϕ_t (upper row) and fiber birefringence L_B (lower row). For simulation the following parameters have been assumed: $\lambda = 632$ nm, $n = 1.456$, $\delta L_T = 5 \times 10^{-7}$/°Cm, $\delta n_T = 1 \times 10^{-5}$/°Cm, $L = 2$ m. Additionally, $L_B = 0.1$ m for upper, $\phi = \pi/4$ rad/m for bottom pictures.

4. Temperature stability of different fiber-optic interferometer configurations

Even though the above changes in SOP may be small, in interferometric interaction described in Section 2, they play a significant role, mainly due to high sensitivity of the system in question. Moreover, the different types of fiber-optic interferometers use various configurations of optical fiber part, and thus their action may be distinctly influenced by fiber birefringence, as has been shown in [14], [16]. Here, the analysis is extended to the case of temperature influence.

The main fiber-optic interferometer system can be divided into in-directional interferometry (IDI) and counter-directional interferometry (CDI), as is shown in Fig. 5. In the first group, the signal and reference beams have the same direction of propagation, whereas they are opposite in the second one. The reason for adopting such a classification has been widely discussed in [16].

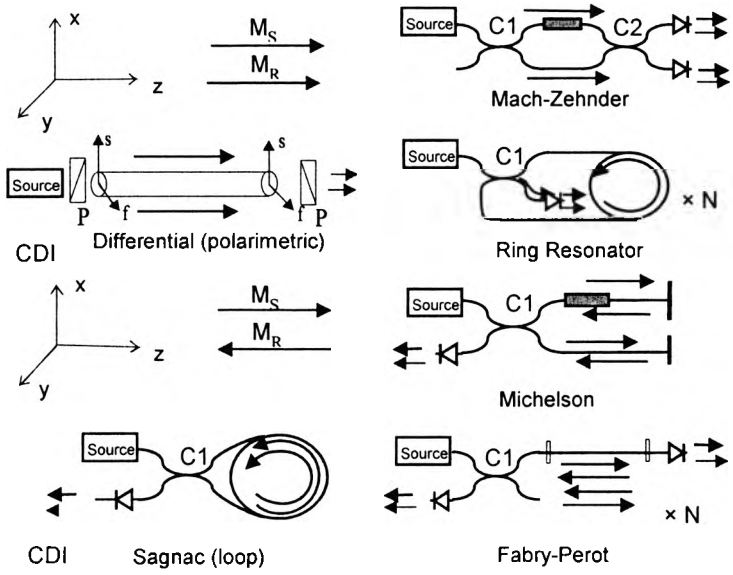

Fig. 5. Classification of fiber-optic interfereometers: IDI – in-directional interferometry system, CDI – counter-directional interferometry system, C1, C2 – couplers, × N – multi-path ways, P – polarizer [16].

Any of the above system descriptions needs to include the fiber-optic coupler, which is assumed as an ideally isotropic 2×2 optical divider. The matrix representation of this element is shown in Fig. 6, and can be written on the basis of [21] as:

$$\mathbf{C}_T = \begin{bmatrix} \exp(-ink_0L) & 0 \\ 0 & \exp(-ink_0L) \end{bmatrix} \begin{bmatrix} \cos KL & 0 \\ 0 & \cos KL \end{bmatrix}$$

$$\equiv D[nk_0\mathrm{L}]\,\mathbf{A}[\cos KL],$$

$$\mathbf{C}_R = \begin{bmatrix} \exp(-ink_0L) & 0 \\ 0 & \exp(-ink_0L) \end{bmatrix} \begin{bmatrix} \sin KL & 0 \\ 0 & \sin KL \end{bmatrix} \begin{bmatrix} e^{-i\pi/2} & 0 \\ 0 & e^{-i\pi/2} \end{bmatrix}$$

$$\equiv \mathbf{D}[nk_0L]\,\mathbf{A}[\sin KL]\,\mathbf{D}[\pi/2] \tag{23}$$

where: K is the coupling coefficient of two optical fibers, L – the coupling length, and matrices $\mathbf{C}_T$ and $\mathbf{C}_R$ stand for the indicated transmission (in Fig. 6, from branch 1 to branch 3) and reflection (in Fig. 6, from branch 1 to branch 4) ways through the coupler, respectively.

As one can see, the coupler action depends on fiber coupling. For an ideal coupler giving equal division between output branches the matrix **A** representing absorber (see Eq. (23)) should be identical for both ways, thus $KL = \pi/4$ plus modulo 2π [21].

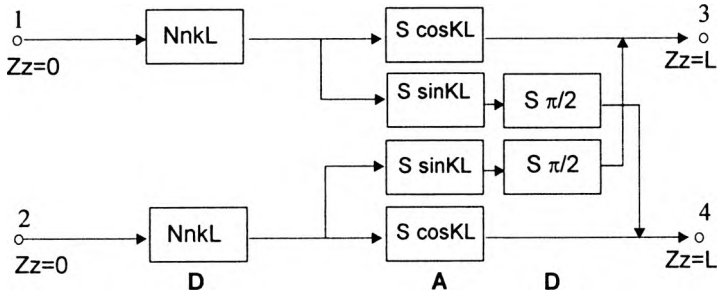

Fig. 6. The Jones marix representation of ideal isotropic fiber-optc coupler. Numbers 1,...4, indicate appropriate coupler branches [21].

The change of temperature introduces changes in fiber length and, generally, affects the coupling ratio. However, owing to the current high technology the commercially available cheap couplers have stable parameters in a wide range from -20 °C to $+60$ °C [28]. For that reason, the thermal effect on fiber-optic coupler has not been taken into account in arm description, and only constant phase shift between two output branches will be considered. This phase shift in interferometry system is the main source of constructive or destructive interference pattern generation, as shown schematically in Fig. 7.

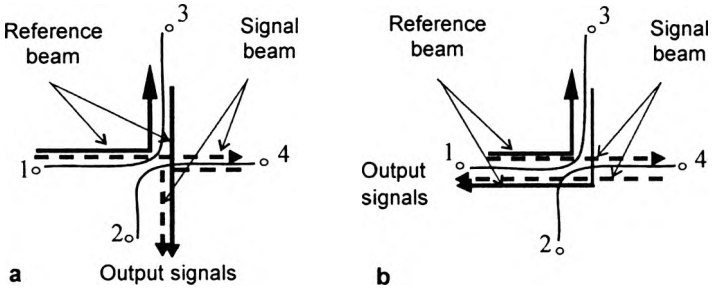

Fig. 7. Schematic view of constructive (**a**) or destructive (**b**) interference pattern as a result of double passing of a signals through the fiber coupler [14].

Applying the above coupler description to the dependence describing fiber optic interference (4) and additionally using relation (21) one can obtain after simple mathematical transformations the following matrix form of the interferometer normalised transfer function [29]

$$I = 0.5[\pm V\cos(\vartheta' + \phi_0)], \quad V = \mathrm{Abs}[m(\Delta T)], \quad \phi_0 = \mathrm{Arg}[m(\Delta T)] \tag{24}$$

where the general complex parameter m

$$m(\Delta T) = E_{\mathrm{in}}^{\dagger}\mathbf{M}_R^{\dagger}(\Delta T)\mathbf{M}_S(\Delta T)E_{\mathrm{in}} \tag{24a}$$

depends on polarisation behaviour of input beam (E_{in}) and temperature dependent reference and signal arms of interferometer (matrices $\mathbf{M}_R$ and $\mathbf{M}_S$), respectively.

In the above notation, sign $(+/-)$ is connected with construtive/destructive interference pattern, V describes scale factor (which is directly proportional to the system sensitivity), while phase coefficient is a sum of measured phase ϑ' generated in a given configuration and additional shift ϕ_0 (bias). The slow time variability of the latter quantity is usually classified as a drift. Moreover, the upper sign † describes the Hermite-conjugate system operation.

To enhance temperature dependent polarisation properties for a given system, the following additional assumption has been made in the further part of this work. Let the reference arm be isotropic (described by a matrix of constant phase retarder $\mathbf{D}(\Delta) = \mathbf{I}\exp(-i\Delta)$ shown as the first matrix in (20)) and assume that reflection in Fabry–Perot and Michelson systems takes place on the tails ended with 100% mirrors (additional phase factor $\exp(-i\pi)$) [16]. Moreover, to obtain only temperature influence, lengths of both interferometer arms are equalised. Theoretically, this can be performed for Mach–Zehnder and Michelson systems under assumption $\Delta = \Delta_S = \Delta_R$. For multiple-beam systems (ring resonator and Fabry–Perot), it is necessary to apply suitable highly coherent sources, because they are in general unbalanced. On the other hand, for two other configurations (balanced systems) high contrast is obtained automatically.

Table. Temperature dependences of the reference and signal paths for the given interferometry configuration in the Jones matrix notation. Additionally, the upper sign T indicates matrix transposition, $\mathbf{In} = \{\{1,0\}, \{0,-1\}\}$ is inversion matrix characteristic for Sagnac interferometer [30], and $^{+)}$ indicates matrix for a simgle pass through the signal arm.

Interfeometer type	Reference path described by $\mathbf{M}_R$ matrix	Signal path described $\mathbf{M}_S$ matrix
Mach–Zehnder	$\mathbf{D}[\Delta]$	$\mathbf{D}[\Delta]\mathbf{R}[\phi_R(\Delta T)-\Phi]\mathbf{G}[\phi_G(\Delta T)]\mathbf{R}[\Phi]e^{-i\vartheta}$
Differential	$\mathbf{D}[-\phi_G(\Delta T)/2]$	$\mathbf{D}[\phi_G(\Delta T)/2]e^{-i\vartheta}$
Michelson	$\mathbf{D}[2\Delta+\pi]$	$\mathbf{D}[2\Delta+\pi]\mathbf{R}^T[\Phi]\mathbf{G}[2\phi_G(\Delta T)]\mathbf{R}[\Phi]e^{-i2\vartheta}$
Sagnac (loop)	$\mathbf{D}[\Delta]\mathbf{In}\mathbf{R}^T[\Phi]\mathbf{G}[\Phi_G(\Delta T)]\mathbf{R}^T[\phi_R(\Delta T)-\Phi]e^{i\vartheta}$	$\mathbf{D}[\Delta]\mathbf{R}[\phi_R(\Delta T)-\Phi]\mathbf{G}[\phi_G(\Delta T)]\mathbf{R}[\Phi]\mathbf{In}e^{-i\vartheta}$
Ring resonator Fabry-Perot (reflection type)	I	$\mathbf{D}[2\pi N]\mathbf{R}[\phi_R(\Delta T)-\Phi]\mathbf{G}[\phi_G(\Delta T)]\mathbf{R}[\Phi]e^{-i\vartheta}$ $^{+)}$
	I	$\mathbf{D}[2\pi N]\mathbf{R}^T[\Phi]\mathbf{G}[2\phi_G(\Delta T)]\mathbf{R}[\Phi]e^{-i2\vartheta}$ $^{+)}$

Applying the above assumptions to the particular optical configuration leads to matrix description of the signal and reference paths in a simple general form given in the Table. The parameter $\Delta = \phi(\Delta T)$, introduced in the Table, indicates isotropic phase shift caused by the light passing through the whole arm of length L, and is equal to the phase described by Eq. (20a). Moreover, for a multiple-beam system a resonance action has been assumed, *i.e.*, a $2\pi N$ phase shift for a single passage through a cavity [16].

The analysis of matrices describing interferometer arms of particular optical configurations has shown that only *differential (polarimetric) system* is insensitive to polarisation properties [14], [16]. This fact is obvious because the idea underlying

construction of this system is based on the polarisation holding fiber (constant phase retarder D with beat length $L_B < 1$ mm represents arms). However, the temperature dependence of differential phase shift (18) affects scale factor but not bias which is stable, as is shown in Fig. 8.

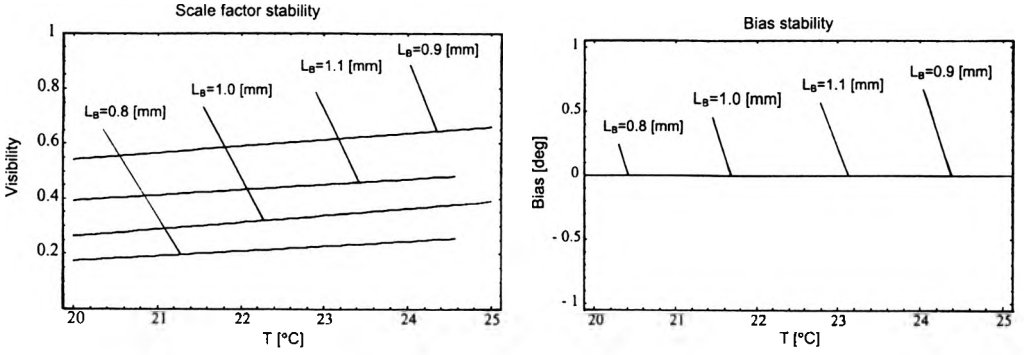

Fig. 8. Temperature influences on differential interferometry action with beat length as a parameter. The optical fiber length $L = 1$ m has been assumed.

In the above simulation the perfect polarizer has been assumed as a part of differential system action. The results obtained are in agreement with those of theoretical analysis of the temperature sensitivity of a fiber-optic polarimeter presented in [31], where it is shown that zero temperature sensitivity may be achieved for certain coating materials of appropriate thickness on fused-silica optical fiber. It should be aluminium for sandwiched construction and copper for non -embedded fiber-optic structures.

Other systems are more or less affected by temperature dependent polarisation changes of of optical fiber used in its arms. Further part of the paper is devoted to a discussion of this problem.

4.1. Two-beam fiber-optic interferometry systems

For the *Mach-Zehnder system*, applying the matrix notation for arms presented in the Table gives the transfer function of the system in the form of (24), where

$$m(\Delta T) = \mathbf{E}_{\text{in}}^{\dagger}\mathbf{R}[\phi_R(\Delta T)-\Phi]\,\mathbf{G}[\phi_G(\Delta T)]\mathbf{R}[\Phi]\mathbf{E}_{\text{in}} \tag{25}$$

stands for the influence of temperature on a given configuration action.

If effects causing rotation of polarisation plane are present only in the fiber ($\mathbf{M}_S = \mathbf{D}(\Delta)\mathbf{R}[\phi_R]$ in Jones description), visibility V and bias ϕ_0 have following temperature dependences:

$$V(\Delta T) = \sqrt{\cos^2\phi_R(\Delta T)+\sin^2\phi_R(\Delta T)\sin^2(2\theta)\sin^2\delta}, \tag{26a}$$

$$\phi_0(\Delta T) = \tan^{-1}[-\tan\phi_R(\Delta T)\sin(2\theta)\sin\delta], \tag{26b}$$

where (θ, δ) are parameters of input light SOP (21b), and $\phi_R(\Delta T)$ is described by relation (20b).

As one can see from (26), a change in sensitivity and drift take place for any input beam SOP. But for linearly polarised input beam ($\delta = 0$), the temperature generates a change in system sensitivity only, without affecting the bias, as shown in Fig. 9**a**,**b**. Generally, this temperature influence is very small (Fig. 9**c**,**d**), but for interferometric measurement where detected changes are extremely small, it might play a significant role.

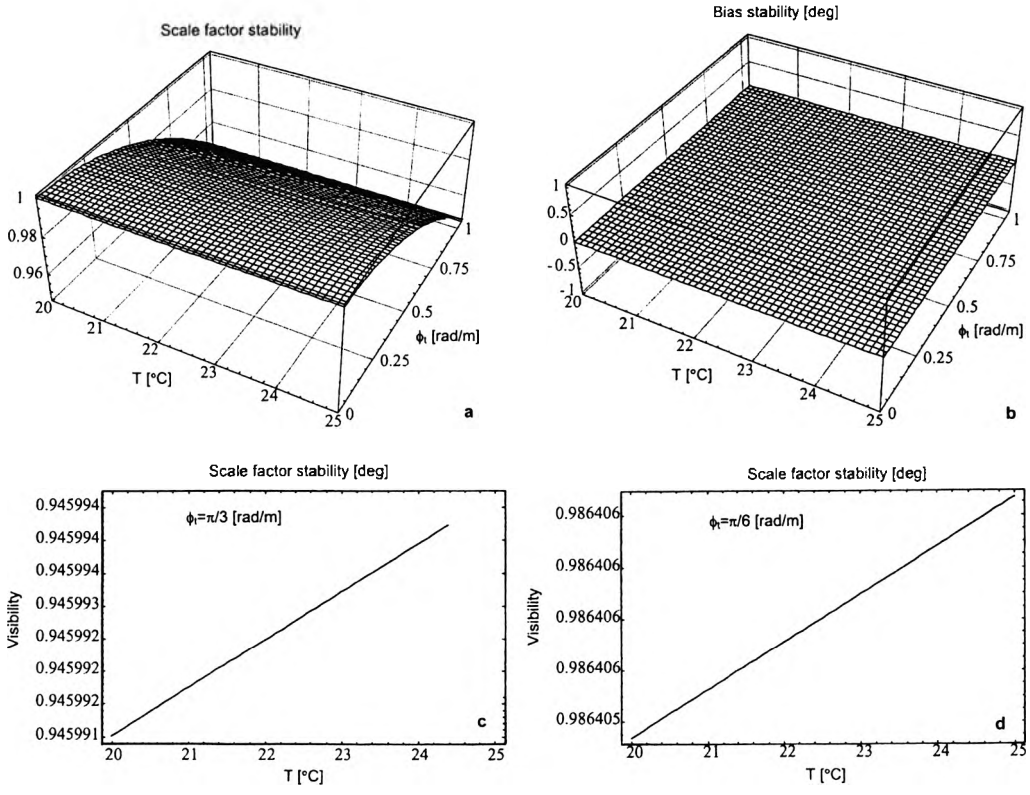

Fig. 9. Sensitivity (**a**, **c**, **d**) and bias (**b**) fluctuations for the Mach–Zehnder configuration with arm lengths $L = 2$ m excited by linear beam in the case of variable temperature. The fiber twist rate $\phi(\Delta T)$ is used as a parameter.

On the other hand, if the system only contains induced linear birefringence ($\mathbf{M}_S = \mathbf{D}(\Delta)\mathbf{G}[\phi_G]$ in Jones description), the respective temperature dependences of the parameters V and ϕ_0 will equal:

$$V(\Delta T) = \sqrt{\cos^2[\phi_G(\Delta T)/2] + \sin^2[\phi_G(\Delta T)/2]\cos(2\theta)}, \tag{27a}$$

$$\phi_0(\Delta T) = \tan^{-1}\{-\tan[\phi_G(\Delta T)/2]\cos(2\theta)\} \tag{27b}$$

where the temperature dependent linear retardation is described by relation (20c).

As one can see, the temperature influence on the Mach–Zehnder system depends on the azimuth of input polarisation θ. According to the results of numerical simulation shown in Fig. 10, in the case of suitable system adjustment, *i.e.*, for uniform excitation of both polarisation modes of the fiber ($\theta = (2n+1)\pi/4$), the temperature dependent fiber birefringence causes the change a sensitivity only. For single mode excitation ($\theta = n\pi/2$) the scale factor is temperature insensitive, while the drift is directly proportional to temperature changes.

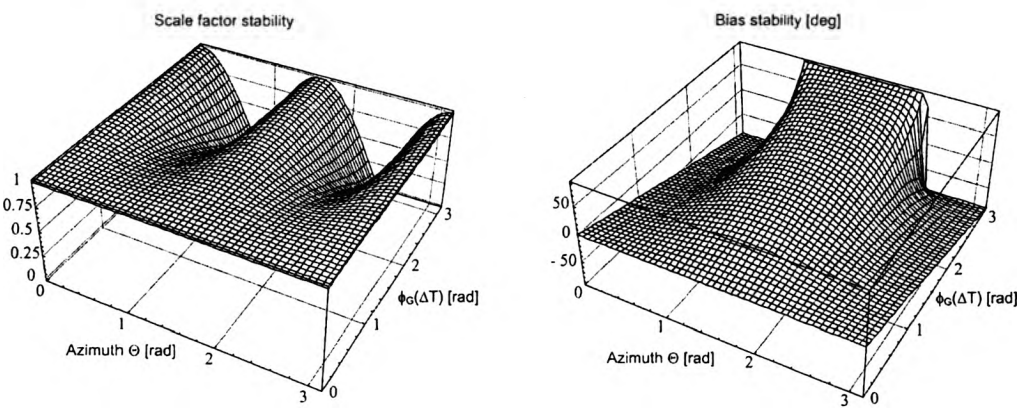

Fig. 10. Sensitivity and bias stability for the Mach–Zehnder system excited by linearly polarised beam with different azimuth in the case of temperature dependent linear birefringence $\phi_G(\Delta T)$ described by relation (20c).

The above situation changes in the case of the *Michelson system*, which is a counter-directional interferometer (CDI). For this interferometer, using the matrix description for arms shown in the Table, one can obtain a system transfer function in the form of (24) where

$$m(\Delta T) = \mathbf{E}_{in}^{\dagger}\mathbf{R}[-\Phi]\mathbf{G}[2\phi_G(\Delta T)]\mathbf{R}[\Phi]\mathbf{E}_{in}. \tag{28}$$

It results from the above notation that in this configuration fiber-optic path can be treated as a classic birefringent plate introducing a temperature dependent retardation $2\phi_G(\Delta T)$, placed at angle Φ with respect to the x-axis of the reference co-ordinate system [10]. Hence, if a path only contains an element introducing rotation of polarisation plane ($\phi_G = 0$, $\mathbf{G}[0] = \mathbf{I}$), one can obtain the following expression:

$$V(\Delta T) = 1, \quad \phi_0 = (\Delta T) = 0, \tag{29}$$

thus this system is temperature independent in the case of existing pure fiber twist. Physically this result is easy to explain because it is due to the fact of both beams

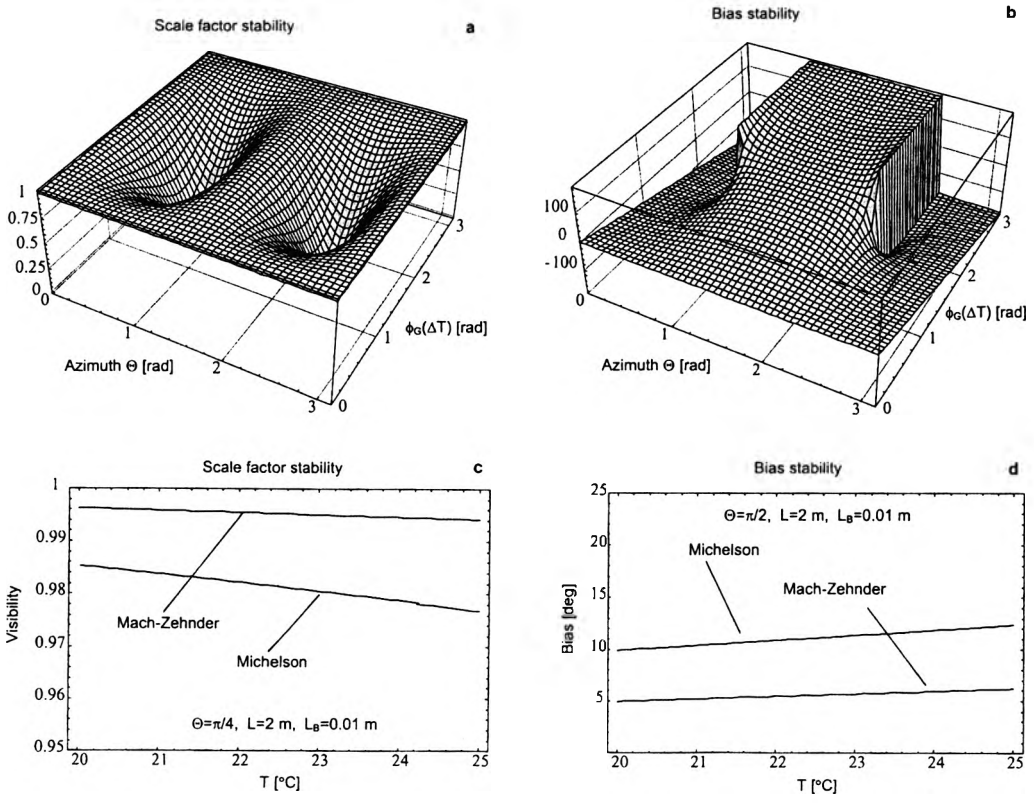

Fig. 11. Sensitivity (**a**, **c**) and bias (**b**, **d**) for the Michelson configuration excited by linearly polarised beam with different azimuth θ and temperature dependent fiber linear birefringence $\phi_G(\Delta T)$.

passing thwice in opposite direction through the same optical fiber. On the other hand, in the presence of linear birefringence only ($\phi_R = 0$, $\mathbf{R}[0] = \mathbf{I}$), the respective expression is

$$V(\Delta T) = \sqrt{\cos^2[\phi_G(\Delta T)] + \sin^2[\phi_G(\Delta T)]\cos(2\theta)}, \tag{30a}$$

$$\phi_0(\Delta T) = \tan^{-1}\{-\tan[\phi_G(\Delta T)]\cos(2\theta)\}, \tag{30b}$$

thus this configuration is twice as sensitive to a temperature change of linear birefringence as the Mach–Zehnder system is (Fig. 11). The character of this sensitivity as a function of input beam SOP is analogous – the system is dependent on the azimuth of input polarisation only.

Note that the last two configurations (the Mach–Zehnder and the Michelson system) have been investigated under assumption of signal and reference arms being equal in length ($L = L_S = L_R$). In such a system, according to the above analysis, it is only temperature dependent birefringence that has influence on its work. Any difference in arm lengths introduces additional bias, which is temperature dependent

as shown by relation (20a). Because the magnitude of this influence is about two orders higher than temperature influences on birefringence induced in optical fiber, thus it may be a more serious problem.

The *fiber-optic Sagnac (loop) interferometer* (FOSI) as a double-beam system includes all configurations discussed so far. This system is CDI as the Michelson system, but it is also balanced (as a differential interferometer, propagation takes place in one optical fiber only). Moreover, the signal path is described by Jones model, in the same way as for the Mach–Zehnder one. The existence of a single coupler in the system causes that distribution of output power is analogous to that for the Michelson configuration.

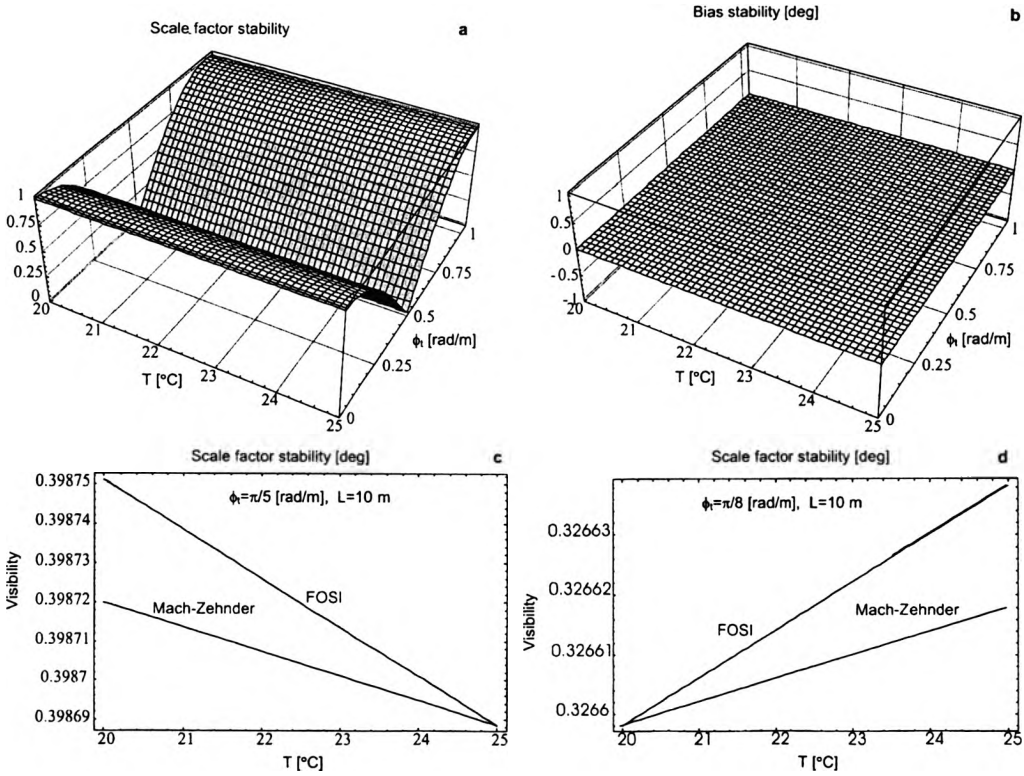

Fig. 12. Sensitivity (**a**, **b**, **c**) and bias (**d**) fluctuations for the FOSI excited by linearly polarised beam in the case of variable temperature. The fiber twist rate ϕ_t is used as a parametr.

According to the matrix description from the Table, one can obtain transfer function in form of (24), if a transducer is placed near to the coupler [29]. In this case parameter m is expressed as

$$m(\Delta T) = E_{in}^{\dagger}\mathbf{R}[\phi_R(\Delta T)-\Phi]\mathbf{G}[-\phi_G(\Delta T)]\mathbf{R}[\phi_R(\Delta T)]\mathbf{G}[\phi_G\Delta T)]\mathbf{R}[\Phi]\mathbf{E}_{in}. \tag{31}$$

It results from the above dependence that if only one factor exists, which causes a rotation of polarisation plane ($\phi_G = 0$, $\mathbf{M}_S = \mathbf{D}(\Delta)\mathbf{In}\,\mathbf{R}[\phi_R(\Delta T)]$, the following simple analytical dependencies can be obtained:

$$V(\Delta T) = \sqrt{\cos^2[2\phi_R(\Delta T)] + \sin^2[2\phi_R(\Delta T)]\sin^2(2\theta)\sin^2\delta}, \tag{32a}$$

$$\phi_0 = \tan^{-1}[-\tan[2\phi_R \Delta T)]\sin(2\theta)\sin\delta] \tag{32b}$$

which exhibit the same character of changes as in the Mach–Zehnder system (see relation (26)). However, the temperature influence for FOSI is twice as big as for the Mach–Zehnder system, which is is shown in Fig. 12.

For the FOSI, thermal dependent circular birefringence causes a rotation of polarisation plane that affects both beams in the same way. Therefore, for the total rotation induced by $\pi/4$ both interacting beams are perpendicular at the output and the sensitivity drops to zero (see Fig. 12**a**). If a total rotation induced angle is equal to $\pi/2$, which is the case of signal vanishing in the Mach–Zehnder system (see Fig. 9), the output beams in the FOSI are rotated by π, being thus parallel, and so the sensitivity is the highest.

On the other hand, if only linear birefringence is observed ($\phi_R = 0$, $\mathbf{M}_S = \mathbf{D}(\Delta)\mathbf{In}\mathbf{G}[\phi_G(\Delta T)]$) from (31) one can obtain the following expression:

$$V(\Delta T) = 1, \quad \phi_0(\Delta T) = 0, \tag{33}$$

which means that the FOSI is insensitive to the pure linear birefringence and their temperature dependencies.

The above special properties of FOSI are caused by the fact that only one fiber is used as a path for both interacting beams. Due to their counter-running propagation, the effect of linear birefringence is neutralised, because independent of the SOP of the excited beam at some arbitrary point along a loop, both beams exhibit the same SOP. According to phenomenological description presented in Section 2, such a situation causes the highest interference contrast.

The unique property of FOSI is its balanced character, which means that signal and reference arm lengths are always equal. This guarantees coherence of interacting beams as well as temperature insensitivity of constant phase retardation observed in Mach–Zehnder and Michelson configuration. Hence, this configuration is similar to the differential system but its sensitivity to external disturbance is by two orders higher, because in this interferometer the disturbance changes optical phase and not the differential one. Comparing the results obtained for the FOSI with those of the Mach–Zehnder shows that FOSI system is more thermally stable. Next, comparing the Michelson system, which reveals temperature dependence of linear birefringence ($\phi_G(\Delta T)$ of an order of $10^{-4} - 10^{-3}$ radian per meter per °C), with the FOSI which reveals temperature dependence of circular birefringence ($\phi_R(\Delta T)$ of an order of $10^{-6} - 10^{-5}$ radian per meter per °C), the latter seems to be more thermally stable, as well.

It is for the above reasons that the FOSI investigations have been the main area of the author's researches in the Applied Physics Division, Institute of Applied Physics, Military University of Technology, Warsaw, Poland, for nearly twenty years, as presented in review paper [32].

4.2. Multiple-beam fiber-optic interferometry systems

The influence of temperature on polarisation properties of fiber-optic path described above is also characteristic for the multiple-beam fiber-optic interferometry system shown in Fig. 5, *i.e.*, the ring resonator and the Fabry–Perot. However, because such systems used multiple crosses through some optical fiber, the form of normalised transfer function in so-called reflection mode of operation for low-finesse system can be written as [33]

$$I = \frac{1 - V\cos[\vartheta' + \phi_0]}{1 + R^2 - 2RV\cos[\vartheta' + \phi_0]} \tag{34}$$

where R stands for the intensity reflection coefficient.

Then the thermal influence on *the ring resonator system* that is IDI can be obtained with good precision from this relation and the matrix form describing its arms shown in the Table. The respective numeric calculation [16], presented in Fig 13, shows that for the ring resonator configuration the effect of temperature influences on polarisation parameters is the same as for the Mach–Zehnder system. The linearly polarised input beam with azimuth $\theta = \pi/4$ has been assumed for calculations.

As one can see, despite of the same character of the temperature influence on particular fiber polarisation parameters (as for the Mach–Zehnder system discussed) the sensitivity of ring resonator to any change of those parameters is distinctly higher. This situation is caused by the peculiarity of a multiple-beam system, *i.e.*, the fact of the light passing many times through the same piece of fiber. It is easy to show that for the ring resonator the vanishing of a signal takes place for as small

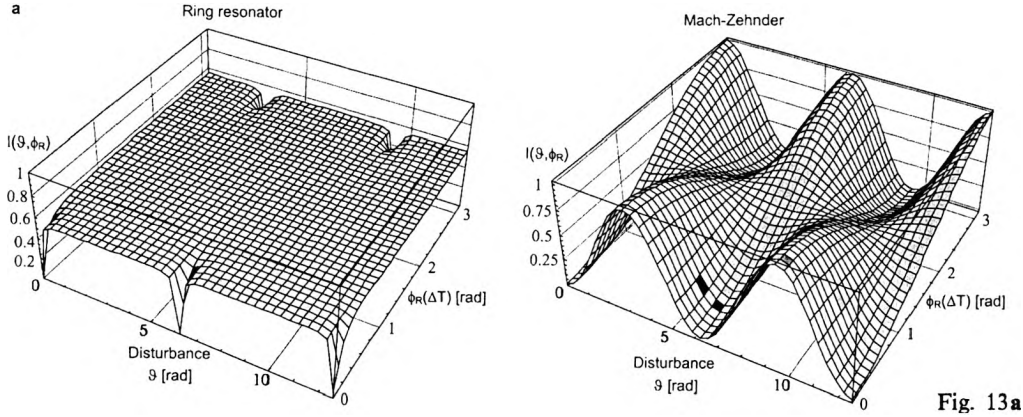

Fig. 13a

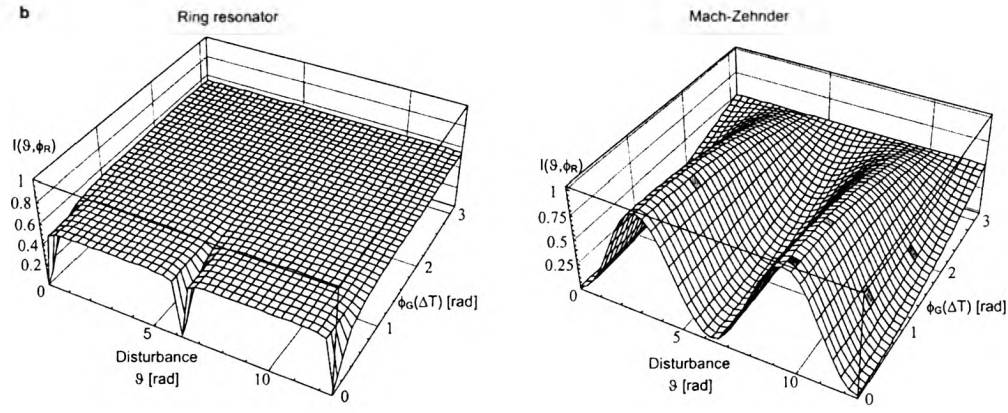

Fig. 13. Comparison between transfer function I of the Mach–Zehnder and the ring resonator for temperature dependent parameters of the signal path; the effect of: **a** – circular birefringence $\phi_R(\Delta T)$, **b** – liner birefringence $\phi_R(\Delta T)$. $R = 0.9$ has been taken in the simulation.

changes in polarisation plane rotation as $\phi_R(\Delta T) = \pi/7$ (or linear birefringence $\phi_G(\Delta T) = \pi/7$), compared with $\pi/2$ for the Mach–Zehnder system. Therefore, the multiple-beam system requires better temperature control, which is usually done by applying the polarisation holding fiber.

The above discussion of the temperature effect on the output signal is also true for the next multiple-beam configuration, *i.e., the Fabry–Perot system* that is CDI. The transfer function of this system may be obtained with good approximation using relation (34) and the matrix description of the signal path $\mathbf{M}_S$ from the Table [14].

An analysis similar to the one for the ring resonator shows that, in this case, the influence of temperature for the circular or linear birefringence (see Fig. 14) produces the same effect on transfer function as for the Michelson system. The peculiarity of multiple-beam configuration is saved. The latter means the existence of thin "areas" of sensitivity to perturbation.

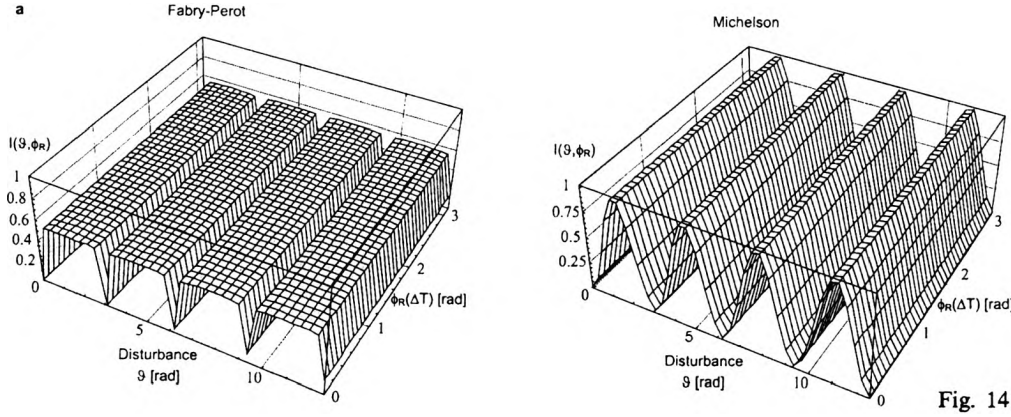

Fig. 14a

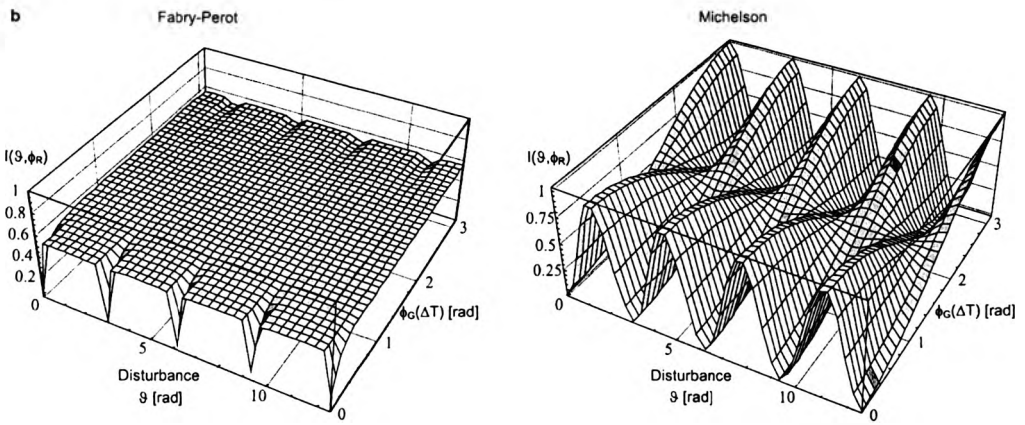

Fig. 14. Comparison of I for the Michelson and the Fabry–Perot systems for temperature dependent parameters of signal path; **a** – circular birefringence $\phi_R(\Delta T)$, **b** – liner birefringence $\phi_G(\Delta T)$. $R = 0.9$ has been taken in the simulation.

In turn, comparing the characteristics of the above multiple-beam interferometers shows that the Fabry–Perot system is less sensitive to SOP disturbances upon temperature changes. Note the double period of transfer function due to the beam passing twice through an optical fiber in the signal path. The existence of the rotation of polarisation plane only, without birefringence, does not change the transfer function. For that reason, the Fabry–Perot configuration should be easier to be subjected to technical realisation.

5. Possibility of the SOP monitoring during interferometer action

The above analysis shows that the SOP of interacting beams in each fiber-optic interferometer is usually temperature dependent, and generates some errors in the system work. Use of polarisation holding fiber is one way of minimising or eliminating this problem, but such a fiber and fiber-optic related elements are very expensive. Hence using the standard single-mode fiber for its construction needs strict temperature control or monitoring the changes of light SOP passing through optical fiber. The second method consists in applying a fiber-optic polarisation analyser connected to a free output end of a coupler used in the interferometer.

The commercially available Hewlett–Packard device HP8509B, giving information about SOP is one, however, very expensive, possibility for such a measurement [34]. Thus, some cheaper in-line versions of the fiber-optic polarisation analyser have been proposed [35]. The first of them, named fiber-optic polarimetric ellipsometer (FOPE), is based on controlled birefringence induced in a piece of standard single-mode fiber. Despite the simpicity of system configuration the FOPE action is thermally unstable [36], because it uses the standard single-mode fiber. Stable temperature operation has been obtained in the second system based on the interferometric Sagnac configuration [37]. The main reason for choosing it is the

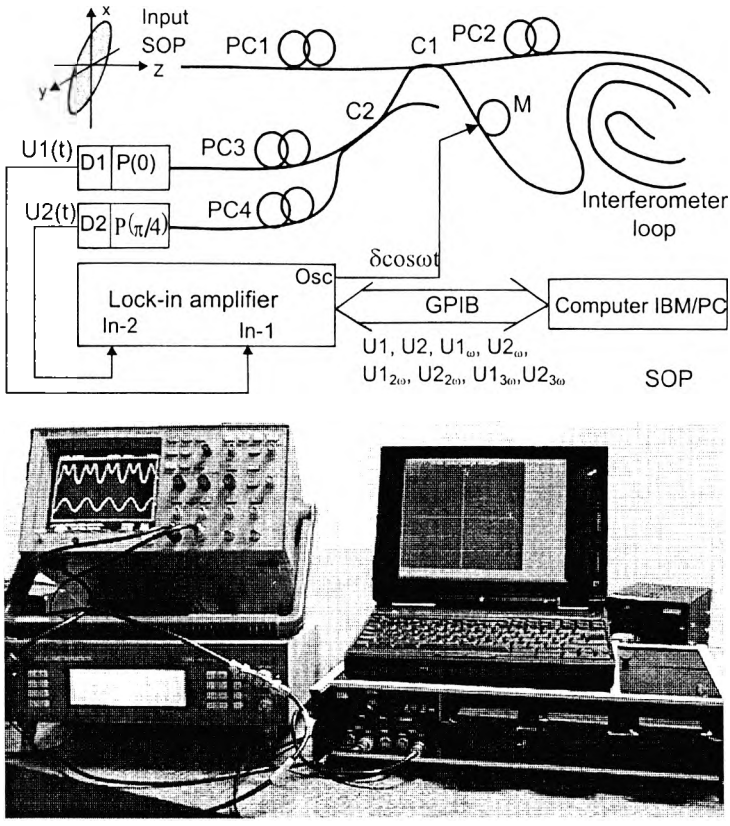

Fig. 15. Construction scheme and general viwe of the FOSE [37].

most stable environmental operation of this interferometer configuration, shown in the previous section. An idea and general view of this device, named FOSE (fiber-optic Sagnac ellipsometer), is shown in Fig. 15. This system, based on the modified FOSI [32], has a double helix coiled loop, the classical fiber-optic phase modulator M, polarizer controller PC2 and input coupler C1, all in the loop. The additional input controller PC1 is used to compensate for birefringence of the input fiber.

Proper operation of the system requires orthonormal SOP of two interfering beams. This is achieved by changing the loop birefringence *via* PC2. The phase modulator M (close to one end of sensor loop) secures the SOP modulation of interfering beams according to the fourth Fresnel–Arago's condition. The additional output coupler C2 splits up the output beam into two parts, which are detected by polarisation sensitive detectors D1 and D2. The PC3 and PC4 are used for the final system adjustment, *i.e.*, to assure 0 and $\pi/4$ azimuth angles of the polarizer P in front of the D1 and D2 with respect to the fast axis of M. The lock-in amplifier detects appropriate harmonics from output signals U1(t) and U2(t), as well as assures suitable driving of M (driving by electrical signal of the type $\delta\cos\omega t$). Finally,

the special numerical software is used to calculate chosen parameters of the polarisation ellipse, *i.e.*, (θ, δ) parameters described by relation (21 a). This programme *via* GPIB interface also controls the proper amplitude of phase modulation $\delta_0 = 2.4048$ (see [37], for details).

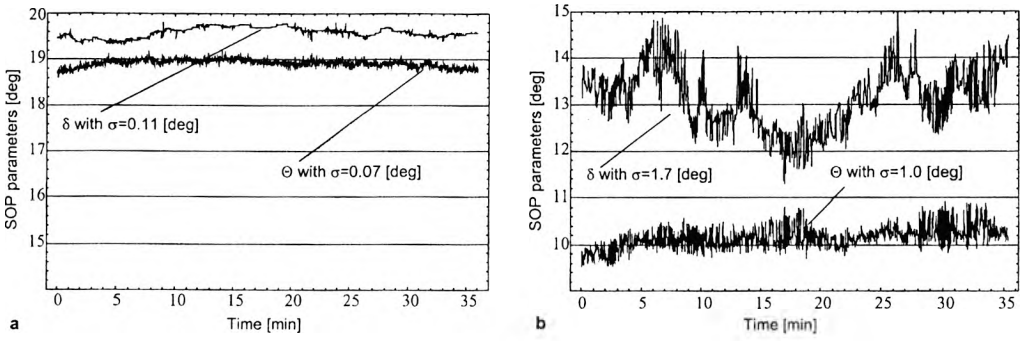

Fig. 16. Stability of the FOSE [38] (**a**), and FOPE [36] (**b**) operation. The input SOP measured by the Babine–Soleis compensator was: $\delta = 19.5$ deg, $\theta = 18.8$ deg and $\delta = 13.5$ deg, $\theta = 9.8$ deg for FOSE and FOPE, respectively.

The system investigations for full polarised light have shown its measurement accuracy equal to 0.09 deg and 0.03 deg for δ and θ, respectively [37]. Recent results obtained for partially polarised light gave 0.11 deg and 0.07 deg for the above parameters [38]. Moreover, as one can see from Fig. 16**a**, the FOSE has a good long-term stability, due to the aspects discussed in Section 4. These results can be compared with the ones obtained for FOPE, as shown in Fig. 16**b**. The comparison of those systems shows FOSE to have the long-term stability by one order better than FOPE.

6. Summary and conclusions

The present description of different fiber-optic interferometry configurations allowed us to reveal basic differences between the bulk and fiber-optic interferometers. Optical fiber and fiber-optic elements in general exhibit variable birefringence. On the contrary, paths of classic interferometers are usually isotropic or constantly birefringent. Therefore, fiber-optic interferometer systems exhibit higher sensitivity to environmental polarisation disturbances. The thermal influence on polarisation properties of fiber-optic interferometer action has been investigated in this paper. Note that it is an important, but not a unique, error source of the fiber-optic interferometer action. Another source of errors are the mechanical vibrations, which has been mentioned in the introduction. Moreover, the instability of commonly used semiconductor optical sources is the next serious error source. Finally, because the fiber-optic interferometer is a complex of different fiber-optic elements connected in-line to form a system, the splice losses (as small as 0.05 dB for fused splice) give

about 0.1 – 0.2% back-reflected signals which are the source of interference error signals. Because they propagate jointly with interfering beams it is very difficult to eliminate them.

The analysis of different configurations shows that particular systems exhibit characteristic features important for application purposes. The most temperature sensitive are Mach–Zehnder and ring resonator configurations. Hence, contrary to bulk optics, the Mach–Zehnder system is rarely applied in practice. There are two main reasons for that. The first one is difficult equalisation of arm lengths. The second one is difficult thermal stabilisation of the system action. On the other hand, the most stable seem to be differential and loop interferometer systems. There are also two reasons for that situation. First, from the construction idea these systems have arms of the same optical length. Second, the same fiber is used as the signal and reference arm, which stabilises working conditions.

The general sensitivity of any configuration to variable arm polarisation properties, shown in Section 4, becomes an important problem that should be solved for any application of fiber-optic interferometer. One of such solutions is to compensate arm polarisation properties by applying a fiber-optic polarisation controller, which allows us to obtain respective system adjustment. However, because it is a passive fiber-optic element, its use does not guarantee compensation thermal changes of birefringence, which generate phase or visibility errors. This means impossibility of measuring unequivocally external disturbances by registering of a change of output intensity only. The general form of transfer function for a given interference configuration (24) contains three variables, *i.e.*, the measured phase ϑ and two SOP parameters (θ, δ). For that reason, unequivocal character of measurement requires also measurements of three independent quantities, for instance, intensity and two parameters describing Jones vector. Such a system is fully polarimetric, in which one can find any phase disturbance by measuring the output intensity and the SOP one can find any phase disturbance.

An example of the system that can be useful for monitoring SOP changes is s the fiber-optic polarisation analyser. Its construction in interferometric configuration has been suggested and described in last part of this paper.

Acknowledgments – The author would like to thank Dr. Ryszard Świłło and Dr. Aleksander Kieżun for their very valuable discussions and comments. This work has been supported by the Polish State Committee for Scientific Research (KBN) under the grant No. 8-T10C-042-19 and MUT PBS-636 statutory activity.

References

[1] TATAM R. P., *Optical Signal Processing: Interferometry*, Sira Workshop, London 1989, 7A-1.
[2] DAKIN J., CULSHAW B., *Fiber Optic Sensor*. Part I, Wiley, London 1989.
[3] KAMINOW I. P., IEEE J. Quant. Electr. QE **17** (1981), 15.
[4] BORN M., WOLF E., *Principle of Optics*, Pergamon Press, New York 1968.
[5] HOCKER G. B., Appl. Opt. **18** (1979), 1445.
[6] HUGES R., PRIEST R., Appl. Opt. **19** (1980), 1477.

[7] GIALLORENZI T. G., BUCARO A. J., DANDRIDGE A., *et al.*, IEEE J. Quantum Electron. QE **18** (1982), 626.
[8] EZEKIEL E., ARDITTY H. J., *Fibre Optic Rotation Sensors and Related Technologies*, Springer-Verlag, New York, 1982.
[9] SCHUETZ L. S., COLE J. H., JARZYŃSKI J., *et al.*, Appl. Opt. **22** (1983), 478.
[10] JONES R. C., J. Opt. Soc. Am. **31** (1941), 488.
[11] IMAI M., OHTSUKA Y., Opt. Quant. Electron. **14** (1982), 515.
[12] IMAI M., OHTSUKA Y., SATOH S., J. Opt. Soc. Am. A **3** (1986), 86.
[13] JAROSZEWICZ L. R., KOJDECKI M. A., Proc. SPIE **2341** (1994), 60.
[14] JAROSZEWICZ L. R., *Polarisation and coherence role in fiber-optics interferometry*, P.L.Q. Thesis, Military University of Technology, Warsaw 1996.
[15] UDD E., *Fiber Optic Sensors*, Wiley, London, 1991.
[16] JAROSZEWICZ L. R, Proc. SPIE **3094** (1996), 204.
[17] TSAO C., *Optical Fibre Waveguide Analysis*, Oxford University Press, New York, 1992.
[18] SAKAI J. I., KIMURA T., IEEE J. Quantum Electron. QE **17** (1981), 1041.
[19] *Ibidem*, **18** (1982), 56.
[20] KAPRON F. P., BORRELLI N. F., KECK D. B., IEEE J. Quantum Electron. QE **8** (1972), 222.
[21] JAROSZEWICZ L. R., J. Tech. Phys. **35** (1994), 289.
[22] MUSHA T., KAMIMURA J-ICHI, NAKAZAWA M., Appl. Opt. **21** (1982), 694.
[23] TATEDA M., TANAKA S., SUGGAWARA Y., Appl. Opt. **19** (1980), 770.
[24] GAUTHIER R. C., Appl. Opt. **35** (1996), 6271.
[25] ZAVRSNIK M., DONLAGIC D., DONLAGIC D., Opt. Eng. **36** (1997), 3200.
[26] PRIMAK W., POST D., J. Appl. Phys. **30** (1959), 779.
[27] AZZAM R. M. A., BASHENA N. M., *Ellipsometry and Polarized Light*, North-Holland, Elsevier, Amsterdam 1977.
[28] *Opto-Link Product Catalog*, Hong Kong 2001
[29] JAROSZEWICZ L. R., KIEŻUN A., [In] A. T. Augousti, N. M. While [Eds.], *Sensors and Their Applications VIII*, IOP Publishing, Bristol and Philadelphia 1997, p. 323.
[30] BURNS W. K., MOELLER R. P., CHEN C-LIN, J. Light. Techn. LT **1** (1983), 98.
[31] MCDEARMON W. B., J. Light. Techn. LT **8** (1990), 51.
[32] JAROSZEWICZ L. R., KIEŻUN A., ŚWIŁŁO R., Appl. Opt. **29** (1999), 139.
[33] SANTOS J. L., LEITE A. P., JACKSON D. A., Appl. Opt. **31** (1992), 7361.
[34] Hewlett-Packard Co., *Lightwave Test and Measurement Catalog*, 1999, p. 435.
[35] JAROSZEWICZ L. R., KIEŻUN A., ŚWIŁŁO R., Proc. SPIE **3746** (1999), 292.
[36] KIEŻUN A., JAROSZEWICZ L. R., Opto-Electron. Rev. **8** (2000), 175.
[37] JAROSZEWICZ L. R., KIEŻUN A., ŚWIŁŁO R., IEICE Trans. Electron. **E83-C** (2000), 384.
[38] JAROSZEWICZ L. R., ŚWIŁŁO R., KIEŻUN A., *Fiber-Optic Sagnac ellipsometer*, submitted to OECC/IOCC 2001 Conf., Australia 2001.

Received May 21, 2001